

# Cooling of hypernuclear compact stars:

Adriana R. Raduta<sup>1\*</sup> Armen Sedrakian<sup>2†</sup> and Fridolin Weber<sup>3,4‡</sup>

<sup>1</sup>*National Institute for Physics and Nuclear Engineering, RO-077125 Bucharest, Romania*

<sup>2</sup>*Frankfurt Institute for Advanced Studies, D-60438 Frankfurt-Main, Germany*

<sup>3</sup>*Department of Physics, San Diego State University, 5500 Campanile Drive, San Diego, CA 92182, USA*

<sup>4</sup>*Center for Astrophysics and Space Sciences, University of California at San Diego, La Jolla, CA 92093, USA*

16 January 2018

## ABSTRACT

We study the thermal evolution of hypernuclear compact stars constructed from covariant density functional theory of hypernuclear matter and parameterizations which produce sequences of stars containing two-solar-mass objects. For the input in the simulations, we solve the Bardeen-Cooper-Schrieffer gap equations in the hyperonic sector and obtain the gaps in the spectra of  $\Lambda$ ,  $\Xi^0$  and  $\Xi^-$  hyperons. For the models with masses  $M/M_\odot \geq 1.5$  the neutrino cooling is dominated by hyperonic direct Urca processes in general. In the low-mass stars the  $(\Lambda p)$  plus leptons channel is the dominant direct Urca process, whereas for more massive stars the purely hyperonic channels  $(\Sigma^- \Lambda)$  and  $(\Xi^- \Lambda)$  are dominant. Hyperonic pairing strongly suppresses the processes on  $\Xi^-$ s and to a lesser degree on  $\Lambda$ s. We find that intermediate-mass  $1.5 \leq M/M_\odot \leq 1.8$  models have surface temperatures which lie within the range inferred from thermally emitting neutron stars, if the hyperonic pairing is taken into account. Most massive models with  $M/M_\odot \simeq 2$  may cool very fast via the direct Urca process through the  $(\Lambda p)$  channel because they develop inner cores where the  $S$ -wave pairing of  $\Lambda$ s and proton is absent.

**Key words:** dense matter – stars: neutron – stars: thermal evolution

## 1 INTRODUCTION

The observations of several white dwarf–pulsar binaries with pulsar masses close to two solar masses (Demorest et al. 2010; Antoniadis et al. 2013; Fonseca et al. 2016; Barr et al. 2017) have spurred intensive research on the problem of hyperonization of dense matter in compact stars. The key issue is the construction of models of compact stars containing hypernuclear matter in their cores, which accommodate the two-solar-mass compact stars mentioned just above. The core compositions of compact stars are computed for a given nuclear equation of state (hereafter EoS). Depending on mass, nuclear densities in excess of several times the density of normal nuclear matter are encountered. So far, the bulk of the research on such stars has been directed towards the integral parameters of non-rotating and rotating compact stars (Weissenborn et al. 2012a,b; Bonanno & Sedrakian 2012; Bednarek et al. 2012; Long et al. 2012; Colucci & Sedrakian 2013; Miyatsu et al. 2013; van Dalen et al. 2014; Gusakov et al. 2014; Maslov et al. 2015; Gomes et al. 2015; Oertel et al.

2015; Fortin et al. 2016; Tolos et al. 2016; Marques et al. 2017).

The purpose of this work is to advance these studies by addressing the problem of their thermal evolution. If the late-time heating processes are ignored then the problem reduces to the neutrino cooling from stellar interior during the time-span  $t \leq 10^5$  yr after the star’s birth, which is followed by asymptotic photon cooling from its surface. The onset of hyperons in dense matter gives rise to an array of new processes involving weak decays of hyperons (and their inverse), such as direct (Prakash et al. 1992) and modified Urca processes (Maxwell 1987; Kaminker et al. 2016). The direct Urca (hereafter dUrca) processes strongly enhance the neutrino luminosity of the star, potentially cooling it very rapidly (Boguta 1981; Lattimer et al. 1991). The required threshold densities of hyperons for these processes to operate are very low, of the order of several percent of the density. Therefore these processes become operative at densities slightly above those where hyperons first become energetically favourable in compact star matter, provided that all involved species are present.

Early models of compact star cooling with hyperon admixtures were studied by Haensel & Gnedin (1994) in the isothermal approximation for non-superfluid hyperons and by Schaab et al. (1998) using a non-isothermal code which

\* E-mail: araduta@nipne.ro

† sedrakian@fias.uni-frankfurt.de

‡ fweber@sdsu.edu

accounted for  $\Lambda$  hyperon pairing. A more recent study by [Tsuruta et al. \(2009\)](#) included also the pairing of  $\Sigma^-$  hyperons along with other additional physics, such as three-body forces in the EoS. Since the onset of hyperons softens the EoS drastically and lowers the maximum mass that can be supported by the EoS, the cooling models mentioned above were built for stars with relatively low masses (e.g., in [Tsuruta et al. \(2009\)](#) the sequences are restricted to  $M/M_\odot \leq 1.7$ ), which are contrary to present-day measurements. On the other hand, the relativistic density functionals (DF) constructed recently provide models of hypernuclear stars which satisfy the presently known constraints from laboratory physics and astrophysics of compact stars. It is, therefore, the purpose of this work to study the cooling of compact stars whose mass range is in agreement with observed data by employing models for the nuclear EoS which account for hyperonic degrees of freedom, and to unveil the new characteristics which hyperonization has on the cooling of compact stars.

This work is structured as follows. In Sec. 2 we first set the stage by describing the covariant DFs on which the EoS used in this work are based. We then go on to solve the Bardeen-Cooper-Schrieffer (BCS) equations in the hyperonic sector to obtain the gaps and critical temperatures for hyperons (i.e,  $\Lambda$  and  $\Xi^{-,0}$ ) interacting via attractive forces. Section 3 is devoted to the discussion of neutrino processes introduced by the hyperonic component; we list the main direct Urca processes on hyperons, as well provide updated rates of the pair-breaking processes on hyperons which account for suppression of the vector current contributions. Section 4 describes the results of our simulations of the thermal evolution of hypernuclear compact stars for three models from our EoS collection. Our conclusions and a concise summary can be found in Sec. 5.

## 2 EQUATION OF STATE AND PAIRING

### 2.1 Density functionals for hypernuclear matter

Hyperons in dense nuclear matter have been studied using a number of methods, ranging from non-relativistic potential based many-body models to Lagrangian based relativistic density functional (DF) methods ([Weber 1999](#); [Sedrakian 2007](#)). The parameters of DFs are fixed by the nuclear phenomenology of hypernuclear matter, nuclear collisions, and compact stars. Non-relativistic potential models ([Balberg & Gal 1997](#); [Baldo et al. 2000](#); [Burgio et al. 2011](#)) fail to produce heavy enough neutron stars (NS) and/or are incompatible with most recent experimental hypernuclear data.

The relativistic DF formalism provides a consistent theoretical framework, which can be used to extrapolate the nuclear EoS to very high densities. In this work we use a set of representative DFs based on the density-dependent parametrization of nucleonic DFs, specifically the DDME2 parametrization ([Lalazissis et al. 2005](#)), and DFs which have constant coupling constants but include non-linear mesonic contributions instead, such as NL3 ([Lalazissis et al. 1997](#)) and GM1 ([Glendenning & Moszkowski 1991](#)). The extensions of the DDME2 model to the hypernuclear sector have been carried out in several works ([Colucci & Sedrakian 2013](#);

Model	$n_s$ [fm $^{-3}$ ]	$E_s$ [MeV]	$K$ [MeV]	$J$ [MeV]	$L$ [MeV]	$K_{\text{sym}}$ [MeV]
NL3	0.149	-16.2	271.6	37.4	118.9	101.6
GM1A	0.154	-16.3	300.7	32.5	94.4	18.1
DDME2	0.152	-16.1	250.9	32.3	51.2	-87.1
SWL	0.150	-16.0	260.0	31.0	55.0	n.a.

**Table 1.** Key nuclear properties of the relativistic DF models considered in this work. Listed are the energy per nucleon ( $E_s$ ) and compression modulus ( $K$ ) at the saturation density of symmetric nuclear matter ( $n_s$ ) together with the symmetry energy ( $J$ ), slope ( $L$ ) and curvature ( $K_{\text{sym}}$ ) of the symmetry energy at  $n_s$ .

[van Dalen et al. 2014](#); [Fortin et al. 2016](#); [Spinella 2017](#)) and we shall use the parametrization of [Fortin et al. \(2016\)](#) and [Spinella \(2017\)](#) below; we shall adopt the parameter set of [Gusakov et al. \(2014\)](#) for GM1A model; for NL3 model we shall employ the parameter set NL3(b) of [Miyatsu et al. \(2013\)](#), which is identical to NL3Yss of [Fortin et al. \(2016\)](#) and very similar to the hyperonic NL3 model of [Wang & Shen \(2010\)](#).

In Table 1 we list the nuclear parameters of these models. Note that, in the NL3 model, the saturation values of the symmetry energy  $J$  and its slope  $L$  are outside of the preferred ranges ([Tsang et al. 2012](#); [Lattimer & Steiner 2014](#)). Nevertheless, we keep this model in our collection for the sake of illustration.

Table 2 displays the properties of the hyperonic stars computed for our collection of EoSs. For each DF the second column lists mesonic fields whereas the third column specifies the underlying flavor symmetry group. The couplings of the  $\sigma$  scalar meson to hyperons,  $g_{\sigma Y}$ , are typically determined from the values of semi-empirical depths of potential wells for hyperons at rest in symmetric nuclear matter at saturation density,

$$U_Y^{(N)}(n_s) = -(g_{\sigma Y} + g'_{\sigma Y} \rho_s) \sigma + (g_{\omega Y} + g'_{\omega Y} n_s) \omega, \quad (1)$$

where  $\rho_s$  is the scalar density, the prime denotes the derivative with respect to the total density; the derivative terms are non-zero only in the models with density-dependent couplings. In all DFs the following values of hyperonic potentials were used:  $U_\Lambda^{(N)} \approx -28$  MeV,  $U_\Xi^{(N)} \approx -18$  MeV and  $U_\Sigma^{(N)} \approx 30$  MeV ([Millener et al. 1988](#)). In the NL3 model ([Fortin et al. 2016](#); [Miyatsu et al. 2013](#); [Wang & Shen 2010](#)), which accounts for the hidden strangeness meson  $\sigma^*$ ,  $g_{\sigma^* \Lambda}$  is determined from the value of the  $\Lambda$ -potential in  $\Lambda$  matter

$$U_\Lambda^{(\Lambda)} = -g_{\sigma \Lambda} \sigma - g_{\sigma^* \Lambda} \sigma^* + g_{\omega \Lambda} \omega + g_{\phi \Lambda} \phi, \quad (2)$$

assuming  $U_\Lambda^{(\Lambda)}(n_s) \approx -5$  MeV ([Takahashi et al. 2001](#)). The couplings with the other hyperons are obtained from symmetry arguments,  $g_{\sigma^* \Sigma} = g_{\sigma^* \Lambda}$  and  $U_\Xi^{(\Xi)} \approx 2U_\Lambda^{(\Lambda)}$ . The vector meson-hyperon couplings constants are expressed in terms of the couplings to the nucleon and assume certain flavor symmetries. The first three DFs in Tables 1 and 2 are based on the SU(6) and the SWL on the SU(3) flavour symmetry. In this last case, the ESC08 model ([Rijken et al. 2013](#)) values are employed for the vector mixing angle  $\theta_v = 37.50^\circ$ , the vector coupling ratio  $\alpha_V = 1$  and the meson singlet to octet coupling ratio  $z = 0.79$ .

Model	mesons	flavor sym.	$n_{\max}$ [fm $^{-3}$ ]	$M_{\max}^Y$ [ $M_{\odot}$ ]	$Y_1$	$n_{Y_1}$ [fm $^{-3}$ ]	$M_{Y_1}$ [ $M_{\odot}$ ]	$Y_2$	$n_{Y_2}$ [fm $^{-3}$ ]	$M_{Y_2}$ [ $M_{\odot}$ ]	$Y_3$	$n_{Y_3}$ [fm $^{-3}$ ]	$M_{Y_3}$ [ $M_{\odot}$ ]	$n_{DU}$ [fm $^{-3}$ ]	$M_{DU}$ [ $M_{\odot}$ ]
NL3	$\sigma, \sigma^*, \omega, \phi, \rho$	SU(6)	0.77	2.07	$\Lambda$	0.28	1.47	$\Xi^-$	0.33	1.73	$\Xi^0$	0.57	2.02	0.21	0.85
GM1A	$\sigma, \omega, \phi, \rho$	SU(6)	0.92	1.994	$\Lambda$	0.35	1.49	$\Xi^-$	0.41	1.67	-	-	-	0.28	1.10
DDME2	$\sigma, \omega, \phi, \rho$	SU(6)	0.93	2.12	$\Lambda$	0.34	1.39	$\Xi^-$	0.37	1.54	$\Sigma^-$	0.39	1.60	-	-
SWL	$\sigma, \omega, \rho$	SU(3)	0.97	2.003	$\Lambda$	0.41	1.51	$\Xi^-$	0.45	1.65	$\Xi^0$	0.90	2.00	0.90	2.00

**Table 2.** Astrophysical characteristics of the relativistic DF EoS models (with hyperons) used in this work:  $n_{\max}$  shows the central densities of the maximum-mass ( $M_{\max}^Y$ ) hyperonic star of each stellar sequence,  $n_{Y_i}$  shows the threshold densities at which hyperons of type  $Y_i$  are produced, and  $M_{Y_i}$  lists the mass of the hyperonic star for that density. The last two entries show the baryon number density ( $n_{DU}$ ) beyond which the nucleonic dUrca process is allowed in purely nucleonic NS matter and the mass ( $M_{DU}$ ) of the associated compact star.

Columns 4-14 of Table 2 list the maximum mass and the corresponding central baryon number density, the threshold density of each hyperonic species and the mass of the star associated with that density. It is seen that for all models the first two hyperons to appear are the  $\Lambda$  and  $\Xi^-$  hyperons; the third type of hyperon to nucleate could be either  $\Xi^0$  or  $\Sigma^-$ . The chosen DFs favour  $\Xi^-$  hyperon over the less massive  $\Sigma^-$  because of its potential in nuclear matter is attractive, whereas that of the  $\Sigma^-$  is repulsive (Millener et al. 1988). Clearly, if the threshold density for appearance of any given hyperon is larger than the central density of the maximum-mass star, that particular hyperon will not be accounted in our simulations. Finally, the last two columns of Table 2 list the baryon number density and NS mass threshold above which the nucleonic dUrca process operates in a purely nucleonic NS matter.

## 2.2 BCS models of hyperonic pairing

The attractive component of the nuclear force between the hyperons will lead to their BCS pairing. Because of the relatively low density of hyperons, the most attractive partial wave is the  $^1S_0$  channel, which would pair hyperons as spin-singlet Cooper pairs. Hyperon-nucleon pairing as well as pairing among non-identical hyperons, e.g.  $\Lambda\Xi^{-,0}$  will be suppressed because of the difference in their densities and/or the difference in their effective masses (Stein et al. 2014). In fact, the latter strongly disfavour cross-species pairing among baryons even when their abundances become equal at some density.

A reliable strategy for computing pairing gaps in nucleonic matter has been outlined in past studies of relativistic DF models of nucleonic pairing, where the non-relativistic BCS equation is solved for a given two-nucleon potential (Kucharek & Ring 1991) using single-particle energies and particle composition computed for the relativistic DF method. Although there is certain inconsistency in the methods of treating the background and pairing correlations, this approach has been validated in computations of finite nuclei within the relativistic Hartree-Fock-Bogoliubov theory (Long et al. 2010).

We employ this strategy and use for the composition of matter the DF results from the previous subsection; for the  $\Lambda\Lambda$  pairing interaction we use the configuration space parametrization of ESC00 potentials (Rijken 2001) given by Filikhin & Gal (2002); for  $\Xi^-\Xi^-$  and  $\Xi^0\Xi^0$  interaction we use the potential designed by Garcilazo et al.

(2016), which corresponds to Nijmegen Extended Soft Core ESC08c potential (Rijken et al. 2013). Our choice of ESC00 and ESC08c potentials is motivated by the fact that they provide maximum attraction in the  $\Lambda\Lambda$  and, respectively,  $\Xi\Xi$  channels. Consequently, our results provide an upper limit on the hyperon pairing and thus maximize the role of hyperon pairing on NS cooling. The  $\Sigma\Sigma$  pairing is disregarded because according to ESC08c potential this interaction channel is repulsive. The pairing in the  $\Lambda$ -channel was studied by Balberg & Barnea (1998) and most recently by Wang & Shen (2010) for a matter composition determined from relativistic DF theory. The  $\Xi$ -channel has been briefly discussed by Takatsuka et al. (2001), but the physical implications of  $\Xi$  pairing has remained largely unexplored.

The quantity determining the onset of superfluidity is the energy gap function  $\Delta_Y(k)$ , obtained by solving the gap equation,

$$\Delta_Y(k) = -\frac{1}{4\pi^2} \int dk' k'^2 \frac{V_{YY}(k, k') \Delta_Y(k')}{\sqrt{[E_{s.p.}^Y(k') - \mu_Y]^2 + \Delta_Y^2(k')}} \quad (3)$$

where  $E_{s.p.}(k)$  is the single-particle energy of hyperon  $Y$  with momentum  $k$ ,

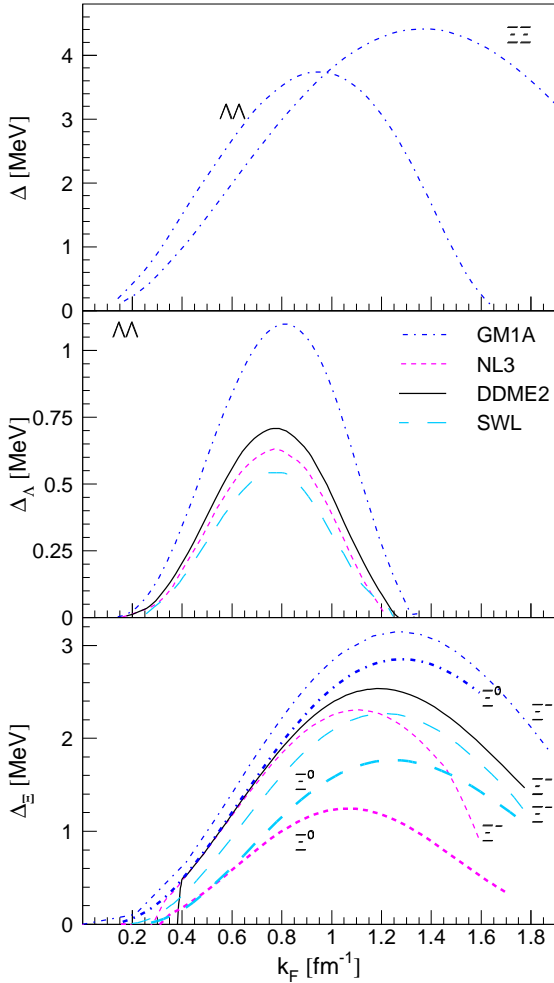
$$E_{s.p.}^Y(k) = \sqrt{(\hbar c)^2 k^2 + m_Y^{*2}} + g_{\omega Y} \omega + g_{\phi Y} \phi + g_{\rho Y} \tau_{3Y} \rho + \Sigma_R \quad (4)$$

where  $\Sigma_R$  represents the rearrangement term entering the models with density-dependent couplings,  $\mu_Y = E_{s.p.}^Y(k_F)$  stands for the chemical potential and  $m_Y^* = m_Y - g_{\sigma Y} \sigma - g_{\sigma^* Y} \sigma^*$  is the Dirac effective mass of the species  $Y$ . For the pairing interaction in the  $^1S_0$  channel the potential matrix element can be written as

$$V_{YY}(k, k') = \langle k | V_{YY} | k' \rangle = 4\pi \int dr r^2 j_0(kr) V_{YY}(r) j_0(k'r) \quad (5)$$

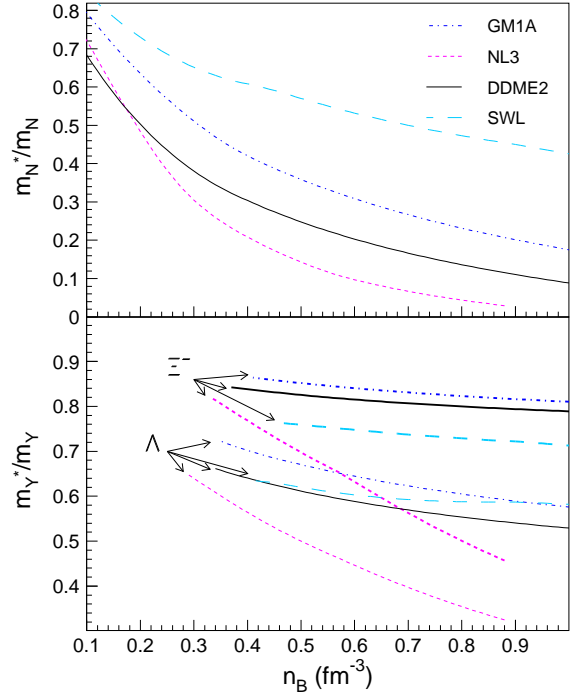
where  $j_0(kr) = \sin(kr)/(kr)$  is the spherical Bessel function of order zero and  $V_{YY}(r)$  is the  $^1S_0$  channel  $YY$  interaction potential in coordinate space. The gap equation (3) was solved numerically by using as an input Eq. (5), with the configuration space interactions for the  $\Lambda$  and  $\Xi$  channels taken from Filikhin & Gal (2002) and Garcilazo et al. (2016), respectively, and for matter properties computed for the models introduced in Sec. 2.1. An iterative method for solving the gap equation was applied with adaptive momentum mesh to account for rapid variations of the integrand in the vicinity of Fermi momentum (Sedrakian & Clark 2006).

Fig. 1 shows the dependence of the pairing gaps for



**Figure 1.** Dependence of  $^1S_0$  pairing gaps at Fermi energy on the Fermi momentum for  $\Lambda$  and  $\Xi$  hyperons in NS matter based on our collection of DF models: (top) gaps obtained with  $m^* = m$  and chemical potentials taken from GM1A model; (middle) gaps for  $\Lambda$  hyperons with medium dependent single particle energies and composition according to DDME2 (solid), NL3 (dashed), GM1A (dash-dotted) and SWL (long-dashed) models; (bottom) same as middle panel, but for  $\Xi^-$  (thin lines) and  $\Xi^0$  (thick lines) hyperons. Note that in the case of DDME2 DF the  $\Xi^0$  hyperon does not nucleate in the density range shown in the figure.

$\Lambda$  and  $\Xi^{-,0}$  hyperons on their respective Fermi momenta. When the dispersive effects are neglected (Fig. 1, top panel) the gaps reflect the attraction in the given channel. The bell-shaped form of these curves results from the increase in the density of states combined with the decreasing attraction among the hyperons as their Fermi momenta  $k_F$  increase. The reduction of the hyperon masses by the medium reduces the density of states, and hence the gap at the Fermi surface. This effect is more pronounced at higher densities where the effective masses are substantially smaller than unity (middle and bottom panels of Fig. 1). The reduction in the  $\Lambda\Lambda$  pairing is larger than in the case of  $\Xi^-\Xi^-$  and  $\Xi^0\Xi^0$  and reflects the magnitude of the change in the effective mass. We have computed also pairing gaps using as a background other DFs, which were recently proposed in the literature, e.g. GM1'B and TM1C from Gusakov et al. (2014) and GM1(c),



**Figure 2.** Dependence of effective masses of neutrons (top panel) and of  $\Lambda$  (thin) and  $\Xi^-$  (thick) hyperons (bottom panel) on baryonic number density, for DF models. The proton and  $\Xi^0$  effective masses are close to those of neutrons and  $\Xi^-$  hyperons as none of our models accounts for  $\delta$ -mesons.

TM1(c) and NL3(c) from Miyatsu et al. (2013), all of which fulfill recent hypernuclear and astrophysical constraints. For these DFs the pairing gaps are comparable or lower than those shown in Fig. 1.

To illustrate the suppression of the pairing gaps by dispersive effects quantitatively we show in Fig. 2 the dependence of the effective masses of baryons on the baryon density for the models studied in this work. The effective masses of baryons decrease with increasing density due to their interactions with scalar mesons. (The NL3 model leads to an unrealistic drop of the effective mass, but this occurs at densities where no stable configurations of compact stars exist.)

The dependence of the pairing gaps on the composition of matter is displayed in Fig. 3. Note that the density range of  $\Lambda\Lambda$  pairing is restricted to densities  $n_B \leq 0.55 \text{ fm}^{-3}$  which implies that at high densities, which may be achieved in massive stars, regions of unpaired  $\Lambda$  matter will exist. In contrast to this, the  $\Xi^-$  component remains paired up to the highest densities. It can also be seen that the NL3 model predicts density ranges for  $\Lambda$ ,  $\Xi^-$  and  $\Xi^0$  pairing, which deviate strongly from other, better constrained models. The largest discrepancy appears for the  $\Xi^0$  pairing range, which is due to the early onset of  $\Xi^0$ s for this model.

### 3 NEUTRINO RADIATION PROCESSES

The neutrino radiation from compact star interiors depends sensitively on the particle content of matter and the magnitude and density dependence of the pairing gaps

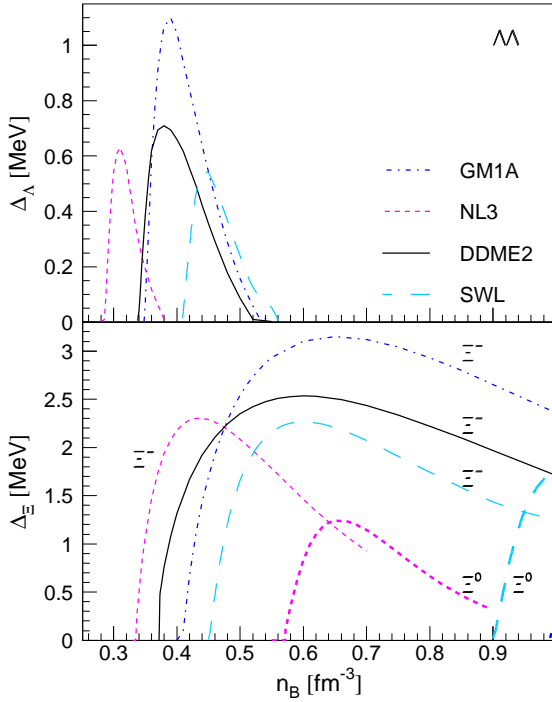
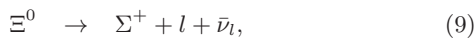
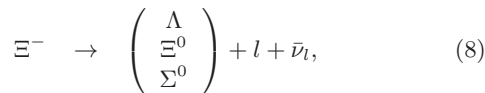
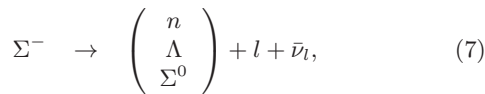


**Figure 3.** The same as in Fig. 1, but for  $^1S_0$  pairing gaps as a function of baryonic number density. Note that the  $\Xi^0$  hyperon appears in the density range shown in the figure only for the NL3 and SWL DFs and its onset for GM1A DF is at  $n_B = 0.99 \text{ fm}^{-3}$ , i.e., close to the upper limit of the range considered.

of fermions. The leading neutrino radiation processes in nucleonic phases are well-known [see for reviews Weber (1999); Yakovlev et al. (2001); Page et al. (2004); Sedrakian (2007)]. The presence of hyperons leads to the hyperonic dUrca processes (Prakash et al. 1992), which can be written symbolically as



where  $l$  stands for a lepton, either electron or muon, and  $\bar{\nu}_l$  is the associated anti-neutrino. Provided that all hyperonic species involved in a given reaction exist in matter, the corresponding thresholds on their density fractions are quite low - of the order of a few percent. The hyperon abundances increase strongly as soon as they become energetically favourable, therefore the hyperonic dUrca processes start to operate soon after the onset of hyperons. Their rates are larger than those of the modified Urca processes involving hyperons (Maxwell 1987) [which can be visualized by adding a bystander baryon to the processes listed in Eq. (6)-(9)]. Although, when allowed by the triangle inequalities (Boguta 1981; Lattimer et al. 1991), the rate of the nucleonic direct Urca process  $n \rightarrow p + e + \bar{\nu}$  is higher than its

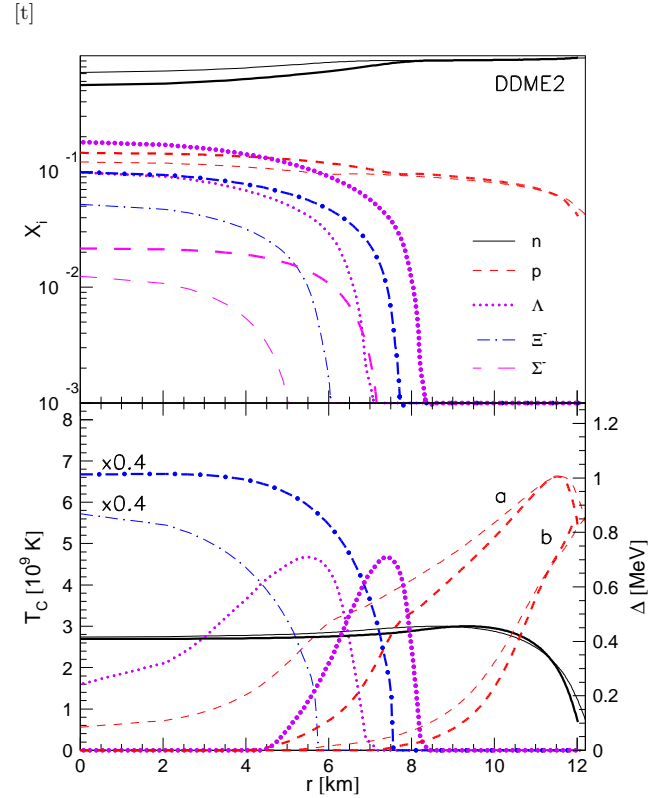
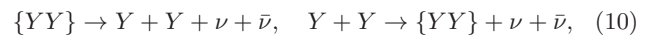


**Figure 4.** Upper panel: composition of NS with masses of  $1.8M_\odot$  (thin) and  $2M_\odot$  (thick lines) in terms of  $n$ ,  $p$ ,  $\Lambda$ ,  $\Xi^-$ , and  $\Sigma^-$  relative abundances, as predicted by the DDME2 Fortin et al. (2016) EoS. Lower panel: the pairing critical temperatures for  $n$ ,  $p$ ,  $\Lambda$ , and  $\Xi^-$  as a function of radial distance from the centre of the star. Two scenarios for proton  $^1S_0$  pairing have been considered: (a) CCDK Chen et al. (1993) and (b) BCLL Baldo et al. (1992). The relation  $T_c [10^{10} \text{ K}] \approx 0.66 \Delta [\text{MeV}]$  has been used to find  $T_c$  for the  $^1S_0$  and  $^3P_2 - ^3F_2$  pairing gaps. The pairing gaps for  $\Xi^-$ s are scaled by a factor of 0.4.

hyperonic counterparts, it is suppressed by the superfluidity of nucleons. Thus, hyperonic dUrca processes dominate if hyperons are not paired. Hyperonic pairing, discussed in the previous section, changes the picture in two-fold way: first, it suppresses the hyperonic dUrca rate (exponentially at low temperatures  $T \ll T_{cY}$ , where  $T_{cY}$  is the critical temperature of hyperonic pairing); secondly, it opens a new channel of neutrino emission based on the Cooper pair-breaking and formation (PBF) mechanism:



where  $\{YY\}$  stand for a hyperonic Cooper pair. The rate of the process (10) has been discussed previously (Yakovlev et al. 1999; Jaikumar & Prakash 2001), but it requires some revision. Specifically, the component of the emissivity to the vector current coupling ( $\propto c_V^2$ ) is negligible for  $S$ -wave paired baryons compared to that of axial-vector coupling ( $\propto c_A^2$ ) (Leinson & Pérez 2006; Sedrakian et al. 2007; Kolomeitsev & Voskresensky 2008, 2010; Steiner & Reddy 2009; Sedrakian 2012). The first contribution scales as  $(v_{YF}/c)^4$ , where  $v_{YF}$  is the Fermi velocity of a given hyperon and  $c$  is speed of light, whereas the second one scales as  $(v_{YF}/c)^2$ . This last contribution can be

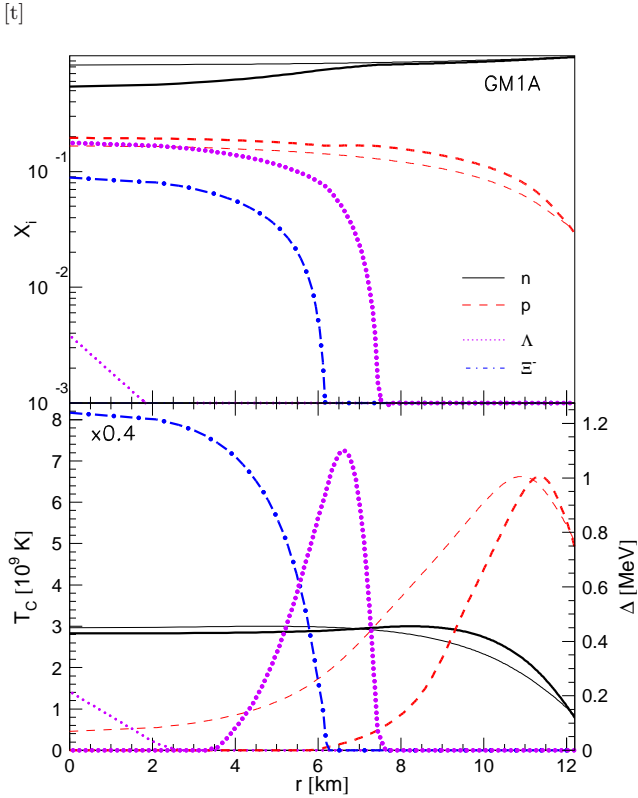


**Figure 5.** The same as Fig. 4, but for NS with masses  $1.5M_{\odot}$  (thin) and  $1.9M_{\odot}$  (thick lines) and the GM1A model (Gusakov et al. 2014). The pairing gaps for  $\Xi^-$ s are scaled by a factor of 0.4. The proton  $^1S_0$  pairing gap is implemented as in Chen et al. (1993) and the neutron pairing gap is chosen as in Fig. 4.

written, in analogy with the result for nucleons, as

$$\epsilon_Y = \frac{4G_F^2 \zeta_A}{15\pi^3 \hbar^{10} c^6} [c_A^2 \nu_0 v_F^2 I_{\nu}]_Y T^7, \quad (11)$$

where the phase-space integral is given by

$$I_{\nu Y} = z_Y^7 \int_1^{\infty} dy \frac{y^5}{\sqrt{y^2 - 1}} f_F(z_Y y)^2, \quad (12)$$

where  $G_F$  is the Fermi coupling constant,  $\zeta_A = 6/7$ , the notation  $[\dots]_Y$  indicates that the quantities in the braces depend on the hyperon type  $Y$ ,  $c_A$  is the axial-vector coupling constant,  $\nu_0 = m_L^* p_F / \pi^2$  is the density of states,  $f_F(x) = [\exp(x) + 1]^{-1}$  is the Fermi distribution function with  $z = \Delta/T$  and  $m_L^*$  refers to the Landau effective mass (as opposed to the Dirac effective mass entering in the definition of eigenstates of the Dirac equation for nucleons and hyperons in medium). Note that we have used the Landau effective masses in expressions for the emissivities of the weak processes. The axial-vector current coupling constants for the tree-level  $Y \rightarrow Y$  transitions are given by Savage & Walden (1997)

$$c_A(\Lambda) = -(F + D/3) = -0.73, \quad (13)$$

$$c_A(\Xi^-) = c_A(\Sigma^-) = D - 3F = -0.58, \quad (14)$$

$$c_A(\Xi^0) = -c_A(\Sigma^+) = -(D + F) = -1.26, \quad (15)$$

$$c_A(\Sigma^0) = D - F = 0.34, \quad (16)$$

where the parameter values used in the numerical evaluation are  $D = 0.79$  and  $F = 0.47$ . Finally we note that the hyperons contribute also to the specific heat of the core of the star; these contributions are suppressed once they pair to form a condensate. The heat capacity and its suppression by  $S$ -wave superfluidity are modelled in full analogy to the  $S$ -wave paired nucleons.

To understand the relative role of the hyperons played in the cooling of NS, it is useful first to examine the relative abundances of the baryon octet  $x_i = n_i/n$ , where  $n_i$  is the partial density of the baryons, and the critical temperatures  $T_{ci}$  of their pairing phase transition as a function of the interior parameter, for example, the internal radius. Figs. 4 and 5 show these dependences for the DDME2 and GM1A models; the results for the SWL model are very close to that of DDME2 and are not shown.

The profiles of the relative abundances reveal that aside from dominant component of neutrons with  $x_n \leq 1$  the baryons separate into two groups: in the first group, which includes  $p$ ,  $\Lambda$  and  $\Xi^-$  the baryon abundances are of the order of 0.1. The second group includes  $\Sigma^-$  and (at high densities)  $\Xi^0$  and, possibly, other hyperons with relative abundances  $\leq 0.01$ . This latter group plays a negligible role in the cooling, except of  $\Sigma^-$  which do not pair under our working assumption that the relevant interaction is repulsive. Among the second group the first baryons to pair are  $\Xi^-$ s. Their maximal critical temperature  $\sim 2 \times 10^{10}$  K; a burst of neutrino emission via PBF processes from this component is overshadowed by the Urca process on  $\Lambda$  hyperons given by Eq. (6). The remaining baryons  $n$ ,  $p$  and  $\Lambda$  thus control cooling through the Urca processes, whereby the following factors play a role: (a) whether or not the nucleonic dUrca threshold is achieved in the star interior; (b) whether some of these baryons lose their pairing at high density leaving some interior regions unpaired. As seen, e. g., from Fig. 4 the more massive star's interior is stripped from  $\Lambda$  and  $p$  pairings, which provides rapid Urca cooling via the  $(\Lambda p)$  channel (see Eq. (6)). Note that the  $\Xi^-$  hyperons are paired in the entire range of their existence and cannot contribute via the dUrca process (except the special case where only the tale of the pairing gap enters the density range of the star).

Thus, we conclude that the main effect of accelerated cooling is caused by absence of pairing in  $p$  and  $\Lambda$  components in the high density regions of the stars: the more massive is the star, the larger is the relevant region. Comparing the two models of dense matter, i.e., Figs. 4 and 5 it is easy to conclude that the same arguments apply also in the case of matter composition based on GM1A model. The minor differences (for example, the absence of  $\Sigma^-$  hyperons, or larger fraction of protons) do not affect the mechanism by which the rapid cooling becomes available with increasing stellar mass.

#### 4 THERMAL EVOLUTION OF HYPERNUCLEAR STARS

The above discussed models of the EoS of hypernuclear matter, which are based on covariant relativistic DF theory, were employed to construct static, spherically symmetrical configurations of self-gravitating objects assuming that these

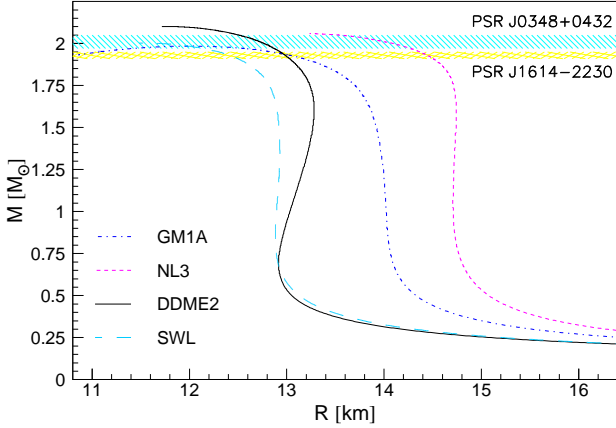


**Figure 6.** Mass versus radius relation for the stellar models considered in this work. The shaded areas show the masses of two massive pulsars, PSR J0348+0432 with  $M = 2.01 \pm 0.04 M_{\odot}$  (Antoniadis et al. 2013), and PSR J1614-2230 with  $M = 1.93 \pm 0.02 M_{\odot}$  (Fonseca et al. 2016).

are non-rotating and nonmagnetized. Fig. 6 shows the mass versus radius relation for our collection of EoS, in particular it demonstrates that our models satisfy the astrophysical constraints placed by pulsar mass measurements.

These models have been further evolved from some initial temperature distribution (chosen to be sufficiently large, but the details are inessential) at initial time assuming that the structure of the models does not change in time. The evolution was followed for  $10^6$  yr after which the star surface temperature drops below the observable limit. We employ the public domain NSCOOL code<sup>1</sup> by D. Page, which was suitably modified to include the physics of hyperonic components. In all considered cases heating sources, magnetic fields and accretion have been disregarded. The envelope is assumed to consist of Fe. The crust EoS of Negele & Vautherin (1973) and Haensel et al. (1989) was smoothly merged with the core EoS. Finally the following computations of the nucleonic pairing gaps are implemented in the code. The neutron  $^1S_0$  pairing in the crust is given by Schwenk et al. (2003). For neutron  $^3P_2 - ^3F_2$  pairing we choose the ‘b’ curve of the gap shown in fig. 10 of Page et al. (2004). Two computations of  $^1S_0$  proton pairing have been used: “CCDK” by Chen et al. (1993) and “BCLL” by Baldo et al. (1992). These computations differ mostly in the density domain that proton superfluid occupies:  $0 \lesssim k_F \lesssim 1.3 \text{ fm}^{-1}$  for CCDK and  $0.1 \lesssim k_F \lesssim 1.05 \text{ fm}^{-1}$  for BCLL. The difference in the maximal values of the critical temperatures for these models is about 20%,  $T_c \approx 6.6 \times 10^9 \text{ K}$  for CCDK and  $\approx 5.6 \times 10^9 \text{ K}$  BCLL.

#### 4.1 Cooling models without nucleonic Urca process

We first discuss models where the process  $n \rightarrow p + e + \bar{\nu}_e$  and its inverse are forbidden by sufficiently low proton fraction.

We start with the cooling models based on the DDME2

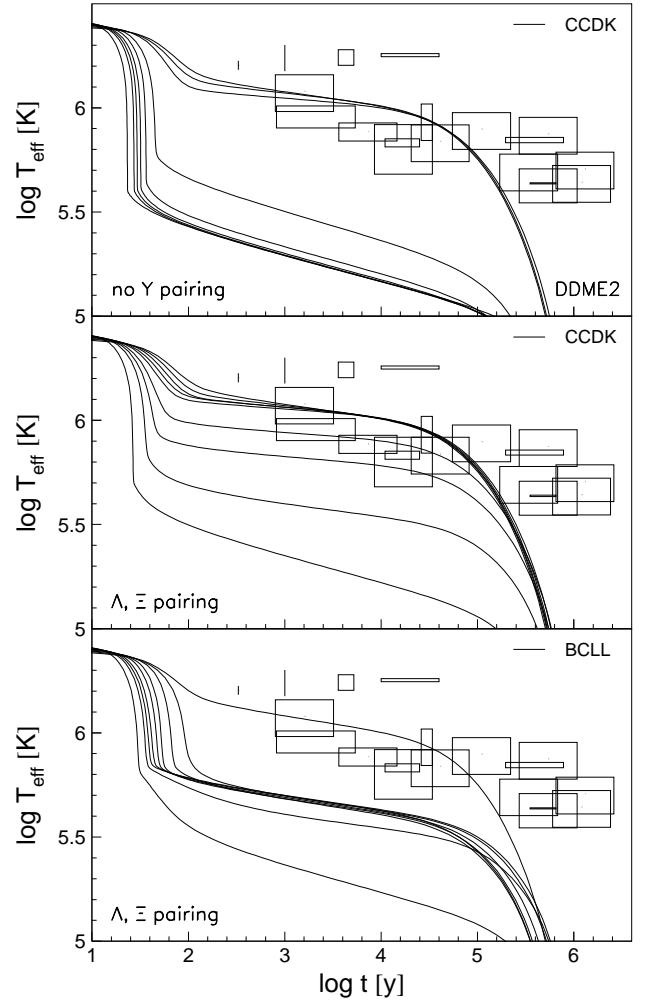


**Figure 7.** Cooling models based on the DDME2 EoS for NS masses 1.3, 1.4, 1.5, 1.6, 1.7, 1.8, 1.85, 1.9 and  $2M_{\odot}$  (from top to bottom) without (top panel) and with (middle and bottom panels) hyperon pairing. Two scenarios for  $^1S_0$  proton pairing have been used: CCDK (Chen et al. 1993) (top and middle panels) and BCLL (Baldo et al. 1992) (lower panel). Observational data correspond to 19 isolated NS listed in Beznogov & Yakovlev (2015).

EoS and show the dependence of the effective surface temperature  $T_{\text{eff}}$  on time in Fig. 7 for the cases of unpaired (upper panel) and paired (middle and bottom panels) hyperon component for the proton pairing model CCDK (Chen et al. 1993). The alternative proton pairing model BCLL (Baldo et al. 1992) with paired hyperon component is shown in the lower panel of the same figure. The data shown in the figure (including the error bars) are the temperatures inferred from the thermal component of the X-ray emission measured from a number of pulsars; the pulsar ages are the spin-down ages unless there is an association with a known supernova [see Beznogov & Yakovlev (2015)].

In the absence of hyperonic pairing the cooling curves for different masses separate into sets corresponding to slowly cooling stars with surface temperatures  $T \sim 10^6 \text{ K}$  and fast cooling stars with surface temperatures by an order of magnitude lower at about  $t \sim 10^4 \text{ yr}$ . This dichotomy

<sup>1</sup> www.astroscu.unam.mx/neutrones/NSCool

can be understood by examining the neutrino luminosity of neutrino processes. For the DDME2 model the threshold for the nucleonic dUrca process is not reached for any model, therefore the only dUrca processes available are those on hyperons. For star masses  $M/M_\odot \simeq 1.5$  the dominant hyperonic process is the dUrca process on  $\Lambda$ s (6) but it is effective only at early stages of evolution (e.g., for  $M/M_\odot = 1.5$  for  $\log t \leq 3.2$  yr) and is suppressed after protons become superfluid. For  $M/M_\odot = 1.6$  model the central density exceeds the  $\Xi^-$  threshold, as a consequence the purely hyperonic Urca process (8) in the  $(\Xi^- \Lambda)$  channel dominates. For  $M/M_\odot > 1.7$  the central density exceeds the  $\Sigma^-$  threshold and another purely hyperonic Urca process (7) in the  $(\Sigma^- \Lambda)$  channel becomes the dominant agent [the process (8) involving  $\Xi^-$  is about 10% of the neutrino luminosity]. Note that the  $\Sigma^-$  decay into neutrons is suppressed by neutron pairing and does not play a role. In the most massive model  $M/M_\odot = 2.0$  the process  $(\Lambda p)$  channel (6) contributes again, because for such massive models the proton pairing vanishes in the inner core ( $r \leq 4$  km).

In the case where the hyperon pairing is included, models fill-in the region between the two extremes discussed above. For stars with  $M/M_\odot \geq 1.7$ , the dUrca process in the  $(\Lambda p)$  channel (6) dominates the early evolution for  $\log t \leq 4$  yr and is suppressed at the later times by pairing. The process (8) in the  $(\Xi^- \Lambda)$  channel does not contribute significantly in any range of masses, because of strong suppression by their superfluidity. For stars with  $M/M_\odot \geq 1.8$  the hyperonic dUrca process (7) involving  $\Sigma^-$ s (which do not pair) is the dominant process up to times  $\log t \leq 5$  to 5.5 yr, after which the photon cooling from the surface takes over. For the massive model with  $M/M_\odot = 2.0$  the inner core ( $r \leq 4$  km) features not only unpaired protons, but also unpaired  $\Lambda$ s. Nevertheless the process (7) dominates, i.e., for massive hyperonic compact stars the dominant cooling is provided by purely hyperonic dUrca process.

The cooling models are sensitive to the proton pairing pattern inside the star because the dUrca process in the  $(\Lambda p)$  channel (6) is the most effective process in low-mass stars. In particular, whenever the proton pairing gaps are small and regions exist where protons are unpaired (see Fig. 4) this process dominates the cooling. This is indeed the case for BCLL pairing, as shown in the lower panel of Fig. 7. Apart from the lightest star, the remaining configurations are effectively cooled by this process, which leads to clustering of cooling curves in the fast cooling regime. In the heaviest stars  $M/M_\odot \geq 1.9$  the competing process on (7) in the  $(\Sigma^- \Lambda)$  channel dominates. In this case the thermal evolution is the same in both models of protonic pairing (c.f. the middle and lower panels of Fig. 4).

Next we consider cooling models based on the SWL equations of state, which are shown in Fig. 8. The difference to the previous case is the absence of unpaired  $\Sigma^-$  hyperons, therefore this model illustrates the physics of cooling of compact stars where *all hyperons pair*. As in the previous case the cooling curves separate into slow and fast cooling sets if hyperon pairing is ignored. The slow cooling set contains two models with  $M/M_\odot = 1.5, 1.6$  which are either purely nucleonic or contain only a small admixture of  $\Lambda$ s. The increase of  $\Lambda$  abundances and the onset of other hyperons accelerates the cooling and the models with  $M/M_\odot = 1.7$  to 2 form the second set of rapidly cooling stars. The  $M/M_\odot = 1.7$

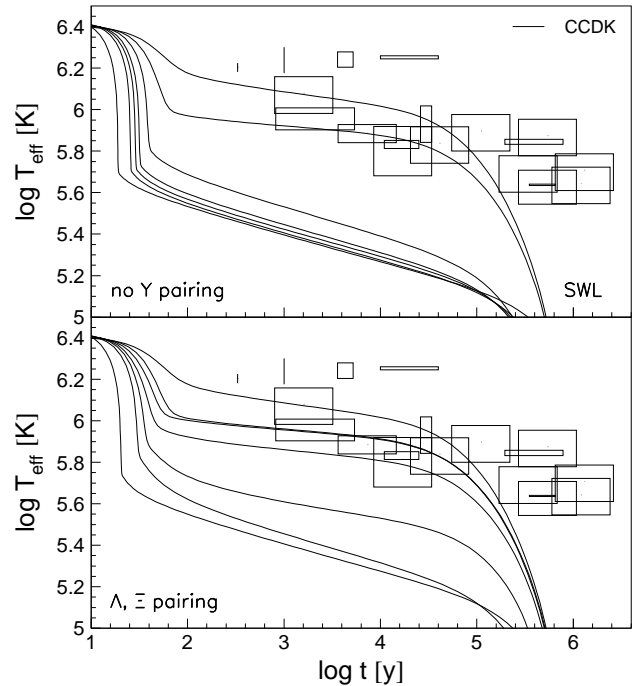


**Figure 8.** Cooling models based on the SWL EoS for NS masses 1.5, 1.6, 1.7, 1.8, 1.85, 1.9,  $2.0M_\odot$  (from top to bottom). For  ${}^1S_0$  proton pairing the CCDK (Chen et al. 1993) gap has been used.

and 1.8 models cool predominantly via the  $(\Xi^- \Lambda)$  channel of Eq. (8), because proton pairing suppresses the former process. For models  $M/M_\odot \geq 1.9$  the proton pairing vanishes in the central region ( $r \leq 4$  km for  $1.9M_\odot$  star) of the star and both processes (6) and (8) contribute nearly equally.

Including the hyperon superfluidity completely suppresses the process (8) on  $\Xi^-$  particles, which have quite large gap. The remaining dUrca process (6) in the  $(\Lambda p)$  channel dominates the neutrino luminosity up to  $\log t \leq 4.5$  for models  $M/M_\odot \geq 1.7$  and 1.8, but its rate is suppressed by the  $\Lambda$  pairing, consequently the cooling tracks pass through the area where the cooler set of the observed stars is located. The models with  $M/M_\odot \geq 1.9$  are not affected by hyperonic pairing, because, as pointed out above, these develop a core where  $\Lambda$  and proton pairing vanish. Thus, we conclude that in the case where  $\Sigma^-$  does not appear in matter *and* cooling via processes involving  $\Xi^-$  are strongly suppressed by their superfluidity the dominant role is played by the dUrca process on  $\Lambda$ s, which provides a good description of the data of the observed cooler compact stars. However, when the cores of most massive stars develop unpaired regions with  $\Lambda$  hyperons and protons the cooling is strongly accelerated and the surface temperatures drop well below the observed ones.

## 4.2 Allowing for nucleonic direct Urca process

Now we turn to the GM1A models, which support the nucleonic dUrca process and consider first the case of unpaired hyperons. The purely nucleonic model with  $M/M_\odot = 1.4$  in this case cools predominantly via the nucleonic dUrca process. For heavier models,  $M/M_\odot = 1.5 - 1.6$ , the dominant neutrino radiation mechanism becomes the hyperonic dUrca

process in the  $(\Lambda p)$  channel, as the nucleonic dUrca process is suppressed by the neutron and proton gaps. For the model with  $M/M_\odot \simeq 1.7$  the cooling is controlled equally by the processes (8) ( $\Xi^- \Lambda$ ) channel and (6) by  $(\Lambda p)$  channel up to time-scales  $\log t \leq 3$  yr after which the last process is suppressed by proton pairing, whereas the first one operates at full strength. Nucleonic dUrca does not play any substantial role in these models during the neutrino cooling era, as it is effectively suppressed by nucleonic pairing. For models with  $M/M_\odot \geq 1.8$  proton pairing vanishes in the inner core ( $r \leq 4$  km for  $M/M_\odot = 1.7$  and  $r \leq 6$  km for  $M/M_\odot = 1.9$ ). As a consequence the hyperonic dUrca process (6) on unpaired  $\Lambda$ s operates at full strength in the  $(\Lambda p)$  channel. Even though protons are unpaired, the neutron pairing suppresses the nucleonic Urca in the neutrino cooling era and it again is unimportant. As seen in Fig. 9, upper panel, the emergence of hyperons leads to lower temperatures of compact stars; for masses in the range below  $1.6 M/M_\odot$ , which is due to dUrca process (6) on  $\Lambda$ s, a stronger shift towards lower temperatures occurs for  $M/M_\odot \geq 1.7$  models due to the onset of the dUrca process (8) on  $\Xi^-$ . The lowest effective temperatures of models with  $M/M_\odot = 1.8$  and  $1.9$  are explained by the fact that, due to the high densities reached in the core, the proton pairing gap in the  $^1S_0$  channel vanishes and, thus, the process (6) operates at full strength over a large fraction of the core.

In the case where hyperon superfluidity is included, the situation is simpler. Because of the large pairing gap of  $\Xi^-$  the dUrca processes (8) on  $\Xi^-$  do not play any role. The nucleonic Urca is suppressed still as in the previous case. The remainder dominant neutrino emission process is dUrca in the  $\Lambda p$  channel (6). As a consequence, the stars with masses up to  $1.8 M/M_\odot$  remain relatively warm through thermal evolution, with their tracks clustered at the lower edge of the observed NS temperatures. The sharp drop in the temperature observed for the model with  $1.9 M/M_\odot$  is due to the unpairing of  $\Lambda$ s at high densities, i.e., the closing of their  $^1S_0$  gap. This occurs in the density range where proton  $^1S_0$  gap closes as well. In the absence of pairing the dUrca process in the  $(\Lambda p)$  channel operates at full strength leading to minimal possible surface temperatures of the most massive models as discussed above.

## 5 CONCLUSIONS

In this work we considered a number of models of hypernuclear matter based on the covariant DF theory which are compatible with the two-solar-mass constraint (Antoniadis et al. 2013; Fonseca et al. 2016) on dense matter and semi-empirical depths of potential wells of hyperons in symmetric nuclear matter at saturation density (Millener et al. 1988). We have solved the BCS equations in the hyperonic sector and obtained the gaps of hyperons in the  $\Lambda$  channel as well as, for the first time, in the  $\Xi^-$  and  $\Xi^0$  channels. With this input, we carried out a series of cooling simulations of compact stars and compared them with the available data.

Our study of the cooling of hypernuclear compact stars reveals that quite generally the hyperonic component plays a dominant role in neutrino cooling of hypernuclear stars, even in the case where the nucleonic dUrca is allowed by

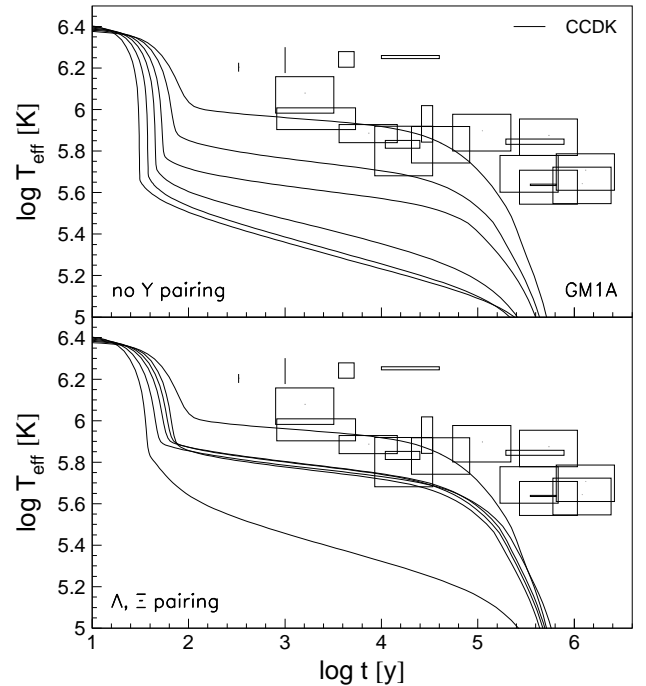


**Figure 9.** Cooling models based on the GM1A (Gusakov et al. 2014) EoS for NS masses  $1.4, 1.5, 1.6, 1.7, 1.8, 1.9 M_\odot$  (from top to bottom). For  $^1S_0$  proton pairing the CCDK (Chen et al. 1993) gap has been used.

the composition of matter. The main cooling agents are various flavours of the hyperonic dUrca process listed in equations (6)-(9). We have included in our studies the pair-breaking processes on hyperons (10), but these turned out to be subdominant to the dUrca processes. The obtained cooling behaviour of our models, shown in Figs. 7-9, depends sensitively on the details of the composition of matter they predict and pairing gaps. In the following we summarize the general trends found from these simulations.

- *Mass-hierarchy.* Consider a sequence of compact hypernuclear stars arranged from the lightest to the heaviest ones. We now follow the changes in their cooling behaviour along such a mass hierarchy. Hyperons start to populate the interiors of compact stars with masses  $M/M_\odot > 1.5$ ; in all models the first hyperons to appear is  $\Lambda$  and the corresponding dUrca process on  $(\Lambda, p)$  plus leptons (see Eq. (6)) is the dominant cooling agent in the neutrino cooling era, even in the case where nucleonic dUrca is kinematically allowed. The efficacy of the dUrca process on  $(\Lambda, p)$  is the result of moderate critical temperature of condensation of  $\Lambda$ s, with a maximum in the range  $T_{c,\max} \simeq 5-7 \times 10^9$  K. For stars with  $M/M_\odot > 1.6$  our models predict the onset of  $\Xi^-$ , which would have provided the dominant cooling mechanism via  $(\Xi^- \Lambda)$  channel of the dUrca process (8) in the absence of hyperonic pairing. However the large critical temperatures of pairing  $T_{c\Xi} \simeq 2 \times 10^{10}$  K prevent  $\Xi^-$ s from playing a role in cooling of the star. For stars with  $M/M_\odot \geq 1.6$   $\Sigma^-$  appear in the DDME2 model, but not in others models. Their appearance implies that the dominant neutrino cooling process is the  $(\Sigma^- \Lambda)$  channel of the dUrca process (7), which accelerates the cooling rate. Finally, a new feature in most

massive stars  $M/M_{\odot} \simeq 2$  is the unpairing of  $\Lambda$ s and protons in the central core of the star, because their large density renders  ${}^1S_0$  pairing interaction repulsive. Then, again, the dUrca process in the  $(\Lambda, p)$  channel (6) dominates the cooling, but at a larger rate characteristic for unpaired hyperonic matter.

- *Hyperonic species.* The  $\Lambda$  hyperon appears first and plays a substantial role when the densities are low enough that the  $\Xi^-$  does not nucleate and when the density is so high that they do not form pairs in the  ${}^1S_0$ . The main neutrino emission channel is the dUrca process (6) in the  $(\Lambda, p)$  channel.

The next hyperon to appear is  $\Xi^-$ . It does not play a role in the cooling, because of its large condensation temperature  $T_{c\Xi} \simeq 2 \times 10^{10}$  K and wide pairing gap. An exception can arise in a narrow mass range around  $M/M_{\odot} \simeq 1.6$ , where the average density of  $\Xi^-$ -gas is low, therefore only the low-density 'tail' of the pairing gap function is important.

The  $\Sigma^-$  hyperon nucleates in one out of three models considered here within sufficiently massive (but stable) hypernuclear stars. If  $\Sigma^-$  do not pair, as implied by a repulsive  $\Sigma^-$  interaction,  $\Sigma^-$  contribute to the dominant cooling mechanism via the  $(\Sigma^- \Lambda)$  channel in Eq. (7). Large neutron pairing throughout the hypernuclear core does not allow for the  $(\Sigma^- n)$  channel to operate.

The fractions of other hyperons, in particular  $\Xi^0$ , never become significantly large in our models to be important for the neutrino cooling.

- *Consistency with the data.* The observational data requires a set of cooling tracks covering the range of temperatures  $5.7 \leq \log T_{\text{eff}}[\text{K}] \leq 6.3$  in the neutrino cooling era  $\log t \leq 5$  [yr]; the required variations of cooling tracks can be achieved by varying the masses of the object along the sequence defined by an EoS. We find that the DDME2 model can account for this, with the lightest stars (featuring hyperonic cores)  $M/M_{\odot} \leq 1.6$  accounting for hotter objects and the more massive ones  $M/M_{\odot} \leq 1.85$  accounting for the cooler objects (see Fig. 7). An important ingredient of this picture is the proton  ${}^1S_0$  gap (CCDK model) extending to large densities; if the proton  ${}^1S_0$  pairing gap is narrow (as exemplified by the BCLL model), then the hypernuclear stars cool too fast. The SWL model shows an analogous behaviour (see Fig. 8). In the case of GM1A model, which allows for nucleonic dUrca process, the cooling of all the models except the most massive one is at the lower edge of the observable band of surface temperatures of thermally emitting NS. Because this model does not feature a  $\Sigma^-$  hyperon, the sharp drop in the temperature for the most massive member shown in Fig. 9 is only due to the unpairing of  $\Lambda$ s and protons at high densities and efficacy of the dUrca process in the  $(\Lambda p)$  channel.

Thus, we conclude that the hypernuclear models where  $\Sigma^-$  hyperon does not nucleate can account for surface temperatures of the cooler class of thermally emitting compact stars and, inversely, hypernuclear stars should be observable in soft X-rays through their thermal emission from the surface, unless they are extremely massive, i.e.,  $1.9 \leq M/M_{\odot} \leq 2$  (see however below).

- *Alternatives.* We now discuss the physical alternatives to the key features discussed above. First, our models are based on the evidence of highly repulsive interaction between  $\Sigma^-$  and nucleons, which has the consequence that the

onset of  $\Sigma^-$  is shifted to higher densities; we also assume a repulsive  $\Sigma^- \Sigma^-$  interaction which allows us to neglect the  $\Sigma^-$  pairing. Should the interaction among  $\Sigma^-$  and nucleons be less repulsive in dense matter  $\Sigma^-$  will replace  $\Xi^-$ s with no significant effect on the EoS. If in addition the  $\Sigma^- \Sigma^-$  interactions are attractive (Sasaki et al. 2015),  $\Sigma^-$  pairing will lead to a suppression of the associated dUrca processes. A study of the consequences of the possible interchange between the  $\Sigma^-$  and  $\Xi^-$  on NS thermal evolution is beyond the scope of the present paper and will be addressed elsewhere. Secondly, the rapid cooling property of most massive models crucially depends on the closing of the  ${}^1S_0$  gaps for  $\Lambda$ s and protons at high densities. However, complete unpairing can be avoided if a higher partial wave channel, such  ${}^3P_2 - {}^3F_2$  coupled channel (which is known to be attractive in the case of nucleons) or even possibly an attractive  $D$ -wave channel, provides sufficient attraction to generate gaps and critical temperatures of relevant magnitude ( $T_c \geq 10^8$  K). In that case the extremely massive hypernuclear stars ( $1.9 \leq M/M_{\odot} \leq 2$ ) will undergo a slower cooling evolution than claimed above.

## ACKNOWLEDGMENTS

AR thanks Constança Providência for discussions and acknowledges the NewCompStar COST Action MP1304 for the partial support of this project through an STSM grant as well as the hospitality of the Frankfurt Institute for Advanced Studies. AS is supported by the Deutsche Forschungsgemeinschaft (Grant No. SE 1836/3-2). FW is supported by the National Science Foundation (USA) under Grants PHY-1411708 and PHY-1714068. We thank ECT\* Trento for its generous hospitality during the final stages of this work.

## REFERENCES

- Antoniadis J., et al., 2013, *Science*, **340**, 448  
 Balberg S., Barnea N., 1998, *Phys. Rev. C*, **57**, 409  
 Balberg S., Gal A., 1997, *Nucl. Phys. A*, **625**, 435  
 Baldo M., Cugnon J., Lejeune A., Lombardo U., 1992, *Nucl. Phys. A*, **536**, 349  
 Baldo M., Burgio G. F., Schulze H.-J., 2000, *Phys. Rev. C*, **61**, 055801  
 Barr E. D., Freire P. C. C., Kramer M., Champion D. J., Berezina M., Bassa C. G., Lyne A. G., Stappers B. W., 2017, *Mon. Not. R. Astron. Soc.*, **465**, 1711  
 Bednarek I., Haensel P., Zdunik J., Bejger M., Mańka R., 2012, *A&A*, **543**, A157  
 Beznogov M. V., Yakovlev D. G., 2015, *Mon. Not. R. Astron. Soc.*, **447**, 1598  
 Boguta J., 1981, *Phys. Lett. B*, **106**, 255  
 Bonanno L., Sedrakian A., 2012, *A&A*, **539**, A16  
 Burgio G. F., Schulze H.-J., Li A., 2011, *Phys. Rev. C*, **83**, 025804  
 Chen J., Clark J., Dave R., Khodel V., 1993, *Nucl. Phys. A*, **555**, 59  
 Colucci G., Sedrakian A., 2013, *Phys. Rev. C*, **87**, 055806  
 Demorest P. B., Pennucci T., Ransom S. M., Roberts M. S. E., Hessels J. W. T., 2010, *Nature*, **467**, 1081  
 Filikhin I., Gal A., 2002, *Nucl. Phys. A*, **707**, 491  
 Fonseca E., Pennucci T. T., Ellis J. A., Stairs I. H., Nice D. J., et al., 2016, *ApJ*, **832**, 167

- Fortin M., Providência C., Raduta A. R., Gulminelli F., Zdunik J. L., Haensel P., Bejger M., 2016, *Phys. Rev. C*, 94, 035804
- Garcilazo H., Valcarce A., Vijande J., 2016, *Phys. Rev. C*, 94, 024002
- Glendenning N. K., Moszkowski S. A., 1991, *Phys. Rev. Lett.*, 67, 2414
- Gomes R. O., Dexheimer V., Schramm S., Vasconcellos C. A. Z., 2015, *ApJ*, 808, 8
- Gusakov M. E., Haensel P., Kantor E. M., 2014, *Mon. Not. R. Astron. Soc.*, 439, 318
- Haensel P., Gnedin O. Y., 1994, *A&A*, 290, 458
- Haensel P., Zdunik J. L., Dobaczewski J., 1989, *A&A*, 222, 353
- Jaikumar P., Prakash M., 2001, *Phys. Lett. B*, 516, 345
- Kaminker A. D., Yakovlev D. G., Haensel P., 2016, *Ap&SS*, 361, 267
- Kolomeitsev E. E., Voskresensky D. N., 2008, *Phys. Rev. C*, 77, 065808
- Kolomeitsev E. E., Voskresensky D. N., 2010, *Phys. Rev. C*, 81, 065801
- Kucharek H., Ring P., 1991, *Z. Phys. A*, 339, 23
- Lalazissis G. A., König J., Ring P., 1997, *Phys. Rev. C*, 55, 540
- Lalazissis G. A., Nikšić T., Vretenar D., Ring P., 2005, *Phys. Rev. C*, 71, 024312
- Lattimer J. M., Steiner A. W., 2014, *Eur. Phys. J. A*, 50, 40
- Lattimer J. M., Prakash M., Pethick C. J., Haensel P., 1991, *Phys. Rev. Lett.*, 66, 2701
- Leinson L. B., Pérez A., 2006, *Phys. Lett. B*, 638, 114
- Long W. H., Ring P., Giai N. V., Meng J., 2010, *Phys. Rev. C*, 81, 024308
- Long W. H., Sun B. Y., Hagino K., Sagawa H., 2012, *Phys. Rev. C*, 85, 025806
- Marques M., Oertel M., Hempel M., Novak J., 2017, *Phys. Rev. C* 96, 045806, ([arXiv:1706.02913](https://arxiv.org/abs/1706.02913))
- Maslov K. A., Kolomeitsev E. E., Voskresensky D. N., 2015, *Phys. Lett. B*, 748, 369
- Maxwell O. V., 1987, *ApJ*, 316, 691
- Millener D. J., Dover C. B., Gal A., 1988, *Phys. Rev. C*, 38, 2700
- Miyatsu T., Cheoun M.-K., Saito K., 2013, *Phys. Rev. C*, 88, 015802
- Negele J., Vautherin D., 1973, *Nucl. Phys. A*, 207, 298
- Oertel M., Providência C., Gulminelli F., Raduta A. R., 2015, *J. Phys. G*, 42, 075202
- Page D., Lattimer J. M., Prakash M., Steiner A. W., 2004, *ApJ Suppl.*, 155, 623
- Prakash M., Prakash M., Lattimer J. M., Pethick C. J., 1992, *ApJ Lett.*, 390, L77
- Rijken T. A., 2001, *Nucl. Phys. A*, 691, 322
- Rijken T. A., Nagels M. M., Yamamoto Y., 2013, *Few-Body Systems*, 54, 801
- Sasaki K., Aoki S., Doi T., Hatsuda T., Ikeda Y., Inoue T., Ishii N., Murano K., 2015, *Prog. Theor. Exp. Phys.*, 2015, 113B01
- Savage M. J., Walden J., 1997, *Phys. Rev. D*, 55, 5376
- Schaab C., Balberg S., Schaffner-Bielich J., 1998, *The Astrophysical Journal Lett.*, 504, L99
- Schwenk A., Friman B., Brown G. E., 2003, *Nucl. Phys. A*, 713, 191
- Sedrakian A., 2007, *Prog. Part. Nucl. Phys.*, 58, 168
- Sedrakian A., 2012, *Phys. Rev. C*, 86, 025803
- Sedrakian A., Clark J. W., 2006, *Phys. Rev. C*, 73, 035803
- Sedrakian A., Muther H., Schuck P., 2007, *Phys. Rev. C*, 76, 055805
- Spinella W., 2017, PhD thesis, Claremont Graduate University/San Diego State University
- Stein M., Sedrakian A., Huang X.-G., Clark J. W., 2014, *Phys. Rev. C*, 90, 065804
- Steiner A. W., Reddy S., 2009, *Phys. Rev. C*, 79, 015802
- Takahashi H., Ahn J. K., Akikawa H., Aoki S., Arai K., et al., 2001, *Phys. Rev. Lett.*, 87, 212502
- Takatsuka T., Nishizaki S., Yamamoto Y., Tamagaki R., 2001, *Prog. Theor. Phys.*, 105, 179
- Tolos L., Centelles M., Ramos A., 2016, *ApJ*, 834, 3
- Tsang M. B., et al., 2012, *Phys. Rev. C*, 86, 015803
- Tsuruta S., Sadino J., Kobelski A., Teter M. A., Liebmann A. C., Takatsuka T., K.Nomoto Umeda H., 2009, *ApJ*, 691, 621
- Wang Y. N., Shen H., 2010, *Phys. Rev. C*, 81, 025801
- Weber F., 1999, Pulsars as astrophysical laboratories for nuclear and particle physics. Institute of Phys., Bristol, U.K.
- Weissenborn S., Chatterjee D., Schaffner-Bielich J., 2012a, *Phys. Rev. C*, 85, 065802
- Weissenborn S., Chatterjee D., Schaffner-Bielich J., 2012b, *Nucl. Phys. A*, 881, 62
- Yakovlev D. G., Kaminker A. D., Levenfish K. P., 1999, *A&A*, 343, 650
- Yakovlev D., Kaminker A., Gnedin O., Haensel P., 2001, *Phys. Reports*, 354, 1
- van Dalen E. N. E., Colucci G., Sedrakian A., 2014, *Phys. Lett. B*, 734, 383